Lawrence Berkeley Laboratory
UNIVERSITY OF CALIFORNIA

Materials & Molecular
Research Division

Submitted to Surface Science

THE SURFACE RECONSTRUCTIONS OF THE (100) CRYSTAL FACES OF IRIDIUM, PLATINUM AND GOLD: I. EXPERIMENTAL OBSERVATIONS AND POSSIBLE STRUCTURAL MODELS

M. A. Van Hove, R. J. Koestner, P. C. Stair,
J. P. Biberian, L. L. Kesmodel, I. Bartoš,
and G. A. Somorjai

January 1980

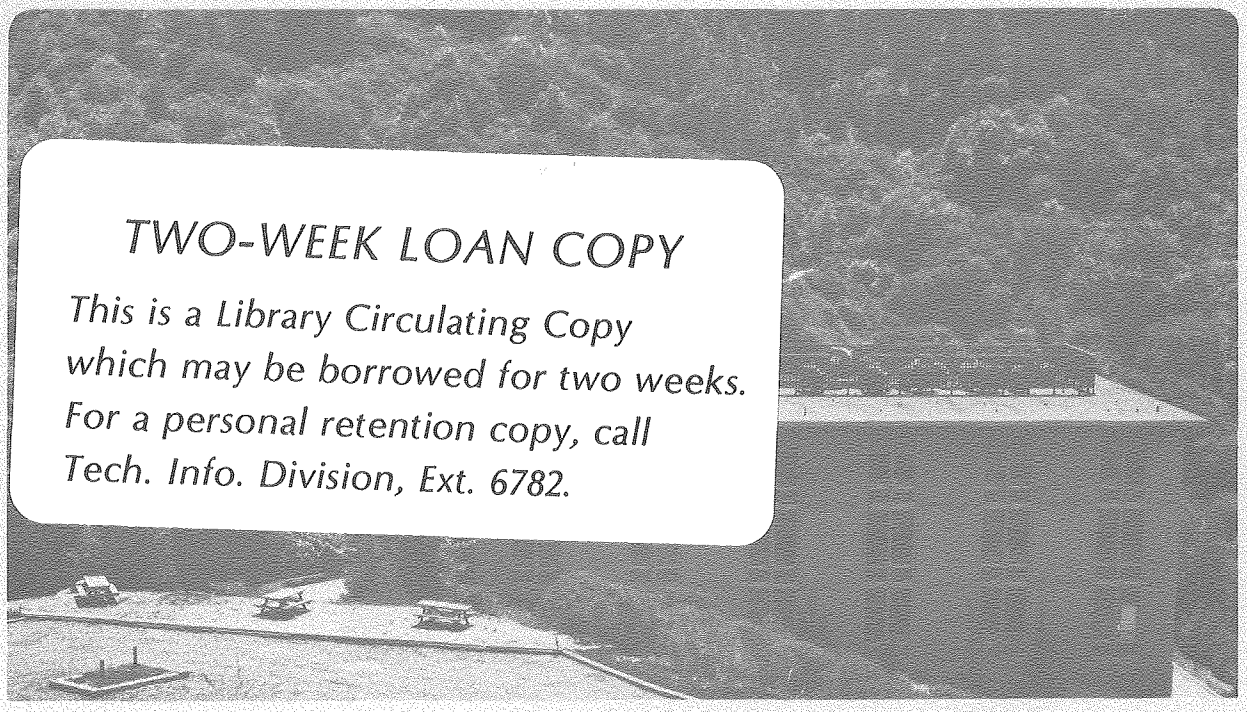

Prepared for the U.S. Department of Energy under Contract W-7405-ENG-48

DISCLAIMER

LBL 10340

THE SURFACE RECONSTRUCTIONS OF THE (100) CRYSTAL FACES OF IRIDIUM, PLATINUM AND GOLD: I. EXPERIMENTAL OBSERVATIONS AND POSSIBLE STRUCTURAL MODELS

M.A. Van Hove, R.J. Koestner, P.C. Stair*, J.P. Biberian,**
L.L. Kesmodel***, I. Bartos****
and G. A. Somorjai

Materials and Molecular Research Division, Lawrence Berkeley Laboratory, and Department of Chemistry, University of California, Berkeley, California 94720

* present address: Department of Chemistry
Northwestern University, Evanston, IL 60201

** permanent address: Centre des Mecanismes de la Croissance Cristalline, U.E.R. Luminy, 70 Route Leon-Lachamp, 13288 Marseille Cedex 2, France

*** present address: Department of Physics, Indiana University
Bloomington, Indiana 47405

**** permanent address: Institute of Solid State Physics, Czechoslovak Academy of Sciences, 16253 Praha 6, Czeechoslovakia

Abstract

The structure of the reconstructed Ir(100), Pt(100) and Au(100) surfaces have been investigated. Low energy electron diffraction (LEED) patterns are analyzed and LEED intensity vs. energy data are measured. A variety of structures is observed by LEED: Ir(100) exhibits a relatively simple (1x5) pattern; Pt(100) shows a series of closely related patterns, a typical representative of which has a $\begin{pmatrix} 14 & 1 \\ -1 & 5 \end{pmatrix}$ structure; Au(100) usually exhibits a c(26x68) pattern, often inaccurately described in the literature as a (20x5) pattern. The reconstruction of Au(111) is also considered for comparison. Various plausible structural models are discussed, while laser simulation is used to lessen the number of these models. The analysis is completed in a companion paper where LEED intensity calculations are reported to determine the atomic locations.

I. Introduction

It has been known for many years, from low energy electron diffraction (LEED) studies, that clean metal surfaces may reconstruct, that is, may have a structure that is not a simple termination of the bulk structure. At present the clean metal surfaces known to reconstruct are the (100) faces of Ir,[1] Pt,[2] Au,[3] V,[4] Cr,[5] Mo,[6] W,[7] the (110) faces of Ir,[8] Pt,[9] and Au[10] and the (111) face of Au.[11] Since many metal surfaces have not been subjected to surface structural studies, surface reconstruction may well be a more widespread occurrence than is apparent at present. Also, only a few surfaces have been studied at low temperatures where the chances for reconstruction are greater than at room temperature (e.g. clean W(100) reconstructs only when cooled). It has been found that some surfaces reconstruct under the influence of adsorbates, such as W(100)[12] and Ni(110)[13] when hydrogen is present. The precise location of atoms in the reconstructed metal surface has been determined only for clean W(100)[14] (which exhibits a c(2x2) superlattice) and Ir(110)[15] and Au(110)[16] both of which have (1x2) superlattices.

The knowledge of the surface structure is of particular importance in studies of surface and bulk phase transitions. The surface structure could correspond to a phase different from the fcc bulk structure, or the surface may act as the nucleation site for a bulk phase transition, just as other defects can. Determination of the reconstructed surface structure is also important for the understanding of the mechanism of phase transitions and to test the theories (such as the soft-phonon theory) proposed to explain their occurrence. Some surface reconstructions have been suggested to be caused by charge density waves [on W(100),[17] Mo(100),[17] Si(111),[18] and 1T-TaS_2(0001)[19]], in which the conduction

electron density has periodic fluctuations with a wavelength a few times the lattice constant, thereby inducing a static wavelike deviation of the atomic equilibrium positions with that same wavelength.

The precise location of atoms in the reconstructed surface must also be known for the analysis of the electronic structure of the metal surface. The existence and the characteristics of surface states depend on the surface structure which also controls the surface density of states. The importance of the surface structure of metals is also evident in the fundamental steps of heterogeneous catalysis since many chemical reactions are known to be surface-structure sensitive. The surface structure also plays an important role in crystal growth and in epitaxy.

In this two part contribution we report a surface structure analysis of the intriguing (100) surface reconstructions of Ir, Pt and Au. We have studied in detail the sometimes complicated LEED patterns for these surfaces, and performed a dynamical LEED intensity analysis of the Ir and Pt(100) reconstructions to determine the atomic locations.

2. Previous observations of the Ir, Pt and Au(100) reconstructions

a. LEED observations

The first clean metal surface reconstructionwas reported in 1965 for the Pt(100) crystal by Hagstrom et al.[2] This metal surface exhibits a so-called "(1x5)"LEED pattern because of the appearance of diffraction beams in(or near)1/5th order positions. In 1967, a Au(100)"(1x5)" reconstruction was observed by Fedak and Gjostein[3] and soon after by Mattera et al.[20] Later in 1967, Fedak and Gjostein resolved a splitting in the LEED spots for Au, leading to a "(20x5)"

rather than "(1x5)" superstructure; they were the first to propose a hexagonal overlayer on the square substrate mesh as a model for the surface rearrangement.[21] In 1969 Palmberg[22] similarly resolved split spots in the LEED pattern of reconstructed Pt(100) and decomposed the pattern into four equivalent domains, each having a $\begin{pmatrix} 13 & 1 \\ -2 & 5 \end{pmatrix}$ unit cell. A single domain was formed by thermal stressing while heating the crystal to or above 1000°C, yielding a straightforward determination of the unit cell. Also in 1969, Grant found that the Ir(100) surface reconstructs and gives a sharp (1x5) LEED pattern without splittings[1], cf. Fig.1.

In 1976, Stair[23] studied the Pt(100) surface reconstruction, arriving at / somewhat different unit cell $\begin{pmatrix} 14 & 1 \\ -1 & 5 \end{pmatrix}$ cf. Fig.2, where the number 14 is an average over values ranging from 13 to 15; a closer look at the diffraction patterns favors a matrix element of about -1.5 rather than -1, yielding a unit cell close to $\begin{pmatrix} 14 & 1 \\ -3 & 10 \end{pmatrix}$. In fact, Blakely reported[24] in 1976 that the reconstruction unit cell in the (100) terraces of a few stepped Pt surfaces depends on the particular stepped surface; in addition, fewer domains are present simultaneously on stepped surfaces. For example, the Pt(13,1,1) surface, with 6-atom wide (100) terraces separated by 1-atom high steps of (111) orientation, has a $\begin{pmatrix} 13.5 & 1 \\ -3 & 6 \end{pmatrix}$ unit cell, better written as $\begin{pmatrix} 27 & 2 \\ -3 & 6 \end{pmatrix}$; the number 6 is possibly due to the width of the 6-atom wide terraces. In the presence of only about 0.02 monolayers of O_2, the Pt(13,1,1) surface facets into a (100) face with a $\begin{pmatrix} 12 & 1 \\ -3 & 5 \end{pmatrix}$ reconstruction unit cell and a (311) facet. The stepped Pt(911) surface, that has 4-atom wide (100) terraces and 1-atom high (111) steps, yields terraces with a $\begin{pmatrix} 12 & 1 \\ -3 & 5 \end{pmatrix}$ reconstruction unit cell. The stepped Pt(510) surface, that also has 4-atom wide (100) terraces, but 1-atom high steps of (100) orientaion, facets to a (100) face again with a $\begin{pmatrix} 12 & 1 \\ -3 & 5 \end{pmatrix}$ reconstruction unit cell and a (210) facet.

Other slightly different surface structures are reported by Heilman et al.[25] and by Norton and coworkers[26] on the clean Pt(100) crystal face. The first authors report a "Pt(100)-hex-R0.7°" reconstruction which we identify with the $\begin{pmatrix} 14 & 1 \\ -1 & 5 \end{pmatrix}$ structure, on the basis of the published LEED pictures which closely resemble those of Stair in the presence of all four domains. They also report a "Pt(100)-hex" structure. If we decompose the published diffraction pattern into four equivalent domains we arrive at a $\begin{pmatrix} 14 & 1 \\ 0 & 5 \end{pmatrix}$ structure, also observed by the second authors. Some of these patterns with their corresponding unit cells are shown in Fig.3. The fact that steps seem to affect the reconstruction unit cell suggests that the detailed form of the reconstruction is influenced by the presence, and especially by the orientation, of surface defects. Similar orientational effects were obtained after sputtering the Pt(100) surface at an angle to the surface normal.[23] The Au(100) diffraction patterns from the (20x5) structure exhibit some triplets of split spots that are not aligned, but have a V shape with an obtuse angle at the apex of the V. Because it was only weakly discernible, this feature was included in a few drawn renditions of the diffraction pattern but not commented upon,[21] although it implies a unit cell different from (20x5). More recent photographs[27,28] obtained when more collimated electron beams were used, show additional split-off spots that clearly have a V or W or longer zigzag arrangement, cf. Figs. 4 and 5. Our best estimate for the unit cell of this structure is a large centered cell labelled c(26x68). Here the number 26 comes from direct measurement of spot separations and is uncertain by about ± 1. The number 68 follows from the angle of the V shape and should be about $\frac{10}{4}x(26\pm1)= 65\pm2.5$; however, the five partly unequal distances between visible spots along the line from the (00) to the (01) spot must be in the proportion n+1:n+1:n:n+1:n+1 with suitable n to produce a coincidence lattice; one then obtains the possible

numbers 2(5n+4), among which the one closest to 65 is 68 with n=7. The number $\frac{26}{2}$=13 corresponds to the often quoted and probably overestimated period 20 in the (noncentered) notation (20x5).

A different structure has also been observed on stepped surfaces of Au with reconstructed (100) terraces. Melle and Menzel[29] report a $\begin{pmatrix} 14 & 1 \\ -1 & 5 \end{pmatrix}$ structure on several such stepped surfaces (observed by RHEED).

Here a comment is necessary concerning the above unit cell designations such as $\begin{pmatrix} 14 & 1 \\ -1 & 5 \end{pmatrix}$ or c(26x68). These designations assume that there is a finite unit cell, that is exclude structures obtained by superposing two incommensurate lattices. The diffraction patterns do not exclude incommensurate lattices, however. The only well-defined quantities are the numbers 5 and 1 in the matrix $\begin{pmatrix} p & 1 \\ q & 5 \end{pmatrix}$ for Pt(100) and in the designation (1x5) for Ir(100) since these are obtained by simple counting of the number of extra spots. All other quantities, such as p and q, and the Au(100) designation, are based on the measured ratio of two lengths in photographs and are therefore uncertain. Only if all these numbers are integers does one obtain a finite unit cell. (Note: the distinction between incommensurate and commensurate lattices becomes pointless from the point of view of LEED for coincidence unit cells larger than the coherence length of the electron beam, which is typically 100Å, but larger in the case of Fig. .4).

b. Observations of Ir, Pt and Au(100) reconstructions by other techniques

Several studies using techniques other than LEED have monitored the Ir, Pt and Au(100) reconstructions. High energy ion scattering has been applied to Pt(100)[30] and Au(100)[31], yielding the information that about one monolayer of the surface atoms are positioned well away from their ideal unreconstructed positions. Also, an ultraviolet photoemission study[32] reveals that the UPS

spectrum of the reconstructed Ir(100) surface resembles more that of Ir(111) than that of unreconstructed Ir(100). Similar results have been obtained on Au(100).[33] Observations with electron energy loss spectroscopy have been made[27] for Au(100) and (111) which also show great similarity between the reconstructed (100) and the unreconstructed (111) surfaces.

It is interesting to note that field ion microscopy studies on Ir, Pt or Au tips have not reported the reconstructions of the (100) surfaces,[34] although a c(2x2) reconstruction on clean W(100) has recently been observed with FIM.[35] This may be due to field effects or to the fact that atomic arrangements are made obvious by FIM only near terrace edges where a reconstruction may either not take place or may not be readily detectable. As pointed out above, reconstructions do occur on some 4-atom wide terraces according to LEED observations.

c. The depth of reconstruction

There is a certain amount of evidence that only the topmost layer of Ir, Pt and Au(100) reconstructs. First, the LEED patterns can be interpreted as a combination of a rearranged top layer and the unmodified square substrate lattice. This presupposes that the attenuation of the substrate contribution by the reconstructed surface layer is not too large; given known electron mean free paths, this can only be true for less than two layers, that is presumably for one reconstructed monolayer. Second, the HEIS results,[28,30] which count the number of displaced atoms, are not consistent with more than one reconstructed monolayer. Of course one cannot exclude small deviations from the substrate geometry in the second layer due to the modified top layer geometry. However, we shall ignore these.

d) Unreconstructed metastable surface structures of the (100) faces of Ir, Pt and Au.

Clean, metastable, unreconstructed (100) (1x1) surfaces have been prepared for Ir,[36] Pt,[37] and Au[27] and the temperature needed to produce an irreversible order-order transition to a reconstructed state has been measured. The unreconstructed Ir(100) surface gradually and continuously reconstructed as the temperature is varied from about 700 K to about 1200 K.[32,36] The resulting (1x5) pattern is stable from 55 to 2100 K.[38] The metastable Au(100)(1x1) surface is converted into the "(20x5)" structure at 373 K.[27] The metastable Pt(100)(1x1) surface transforms into the "(20x5)" structure at 400 K,[37,39] but upon further heating to 1100-1150 K it is converted into the "Pt(100)-hex-R0.7°" structure mentioned above.[39] The latter structure is stable from 77 to 1450 K.[39]

e) Previous structural analyses

No full dynamical LEED analysis of the reconstructed Ir, Pt or Au(100) surface structures has been published. However, a double-diffraction LEED calculation has been attempted in the case of Pt(100), that assumed the presence of a hexagonal top monolayer. A certain degree of agreement between experiment and theory has been achieved.[39] Dynamical (spin-polarized) LEED calculations have been performed for the unreconstructed metastable surface structures of Pt and Au(100)[40] which yield good agreement with experimental IV curves when an ideal, unrelaxed surface was assumed; no relaxations of the surface atoms were considered. From past experience with similar studies one may assume that for this case the topmost layer spacing has the bulk value within about 5%. A HEIS result for metastable Pt(100)(1x1) indicates a minimal outward relaxation of this spacing by $0.5 \pm 0.5\%$.[30]

3. LEED intensity measurements

An Ir crystal (10 ppm impurities, Lot#6666, Orion Chemical Co.) was oriented and spark cut to within $\frac{1}{2}°$ of the (100) plane; it was then polished to a .5 μm diamond paste. The Pt crystal (1 ppm impurities, Materials Research Corp.) was similarly oriented and spark cut, then polished to a .5 μm alumina grit. The crystals were spotwelded to a Ta foil (for the Ir crystal) or a Pt foil (for the Pt crystal) mounted on a modified Varian manipulator. The "flip" mechanism, commercially available, was modified to allow azimuthal rotation of the crystal without changing the polar angle.

Both crystals were cleaned by a combination of Ar^+ bombardments and oxygen treatments. Calcium / proved to be the most troublesome impurity; it was depleted from the near surface region by repeated heating (occasionally in the presence of O_2)/Ar^+ bombardment cycles. Heating the crystal would draw Ca to the surface, the segregation becoming more dramatic with ambient O_2 present, and the Ar^+ bombardment would remove the surface Ca. Small C concentrations stabilized the unreconstructed Pt and Ir(100) surfaces; a light O_2 treatment [10-20 minutes, 800°C (for Pt crystal) or 1000°C (for Ir crystal), 1-5x10^{-7} torr] would remove this residual carbon yielding sharply focused, intense Ir(100)-(1x5) and Pt(100) $\begin{pmatrix} 14 & 1 \\ -1 & 5 \end{pmatrix}$ LEED patterns with low background intensity.

Photographs of the Pt(100) $\begin{pmatrix} 14 & 1 \\ -1 & 5 \end{pmatrix}$ and Ir(100)-(1x5) LEED patterns were taken within a 10 minute interval at a base pressure ∿1x10^{-9} torr with the crystal temperature falling from ∿50°C to ∿30°C. (CO had just been flashed off the crystal by heating to 600°C (for Ir) or 900°C (for Pt).) A Nikon F camera equipped with 85 mm lens, K2 + K3 +K4 extension rings, and motor drive, was used; the film used was Kodak's Pan-X 2484. The Pt LEED pattern was photographed at polar angles θ = 0°, 4°, 10°, 16° with azimuth θ = 45° (θ=0° being defined as

a [011] direction) in 2 eV steps stretching from 10 - 100 eV; the components in the Pt(100) $\begin{pmatrix} 14 & 1 \\ -1 & 5 \end{pmatrix}$ split spots were measured separately. The Ir LEED pattern was photographed at polar angles $\theta = 0°$, 10°, 20° with azimuth $\phi=0°$ in 2 eV steps from 20 - 200 eV. Only photographs of LEED patterns for one crystal orientation (for example $\theta=10°$, $\phi=0°$) with the specified energy range (for example, 120 - 200 eV) were taken during the 10 minute interval. The crystal was then recleaned before another set of photographs were taken; the major contaminant after photography was C, probably produced by LEED beam fragmentation of the adsorbed CO from the ambient.

The film was developed using DuPont extra fast X-ray developer. The developing, fixing, and washing times were all 150 seconds at 28.5°C. The processed film was scanned using a computer-controlled, digital output, stepping microdensitometer with the output transferred to a magnetic tape. About 120 density measurements were taken for a reasonably sized LEED spot on the film image. The tape was later analyzed by a computer program which calculated the intensity of each diffraction spot within the scanning boundary during microdensitometry; these intensities were normalized in the computer program by dividing the photographically measured spot intensities with the LEED beam currents recorded just after photography. Comparing the Ir and Pt I-V profiles, the Ir curves have more gaps, appear noisier, and have larger scaling factors; the major reason for this discrepancy is the shutter speed being limited to about 1/4 sec in the Ir data, rather than 1 sec as in the Pt data.

4. Interpretation of the diffraction patterns

Ir(100)

The diffraction pattern of the reconstructed Ir(100) surface implies

the presence of a (1x5) unit cell. There are no systematic absences or weaknesses of any of the (1x5) spots. This fact puts some restrictions on possible models, such as the absence of glide symmetry planes or domain structures (within the electron coherence length). However, it leaves open many options for the relative positions of the surface atoms within the unit cell since the unit cell has an area that is sufficient to accommodate up to 6 atoms in one plane. One possibility is a hexagonal top layer, as illustrated in Fig.6. The hexagonal layer, if it is planar, must be contracted in the 5-fold direction by 3.92% to fit on the substrate in the (1x5) unit cell. Other possibilities will be discussed in the next section.

Au(100)

The reconstructed Pt(100) and Au(100) diffraction patterns are more complicated. Figure 5 shows a diagram of the diffraction pattern[27,28] due to one domain of reconstructed Au(100). It implies a c(26x68) unit cell structure of the surface which is approximated by a (20x5) unit cell in poorly resolved LEED patterns. Many of the possible diffraction spots, based on the c(26x68) unit cell, are not detected. Such a large unit cell can be understood as one large domain that consists of many (1x5) units identical to those of Ir(100)(1x5). The regular repetition of the domains produces the splitting of the 1/5th order spots due to the (1x5) units. It is necessary to assume (1x5) units within the domain to obtain significant intensity near the 1/5th order positions of the diffraction pattern. If we indeed have a domain structure, the individual split-off components of each 1/5th order spot should have an almost identical energy dependence of their intensiti es, except for constant factors. This is because such split spots can be regarded as the product of the (1x5) diffraction pattern,

with its complicated energy dependence of intensities, and the c(26x68) superlattice pattern, which in itself produces only a smooth energy dependence of intensities. However, one can observe in the experiment that the split spots do not exhibit similar intensity changes as the electron energy is varied; for example, there are reversals in the intensities of neighboring split spots. Therefore, the simple domain model of (1x5) units is incorrect.

A different interpretation of the c(26x68) periodicity comes about when one tries to understand the diffraction pattern with its many absent spots in terms of multiple scattering effects. The combination of a suitable hexagonal lattice and the square lattice of the unreconstructed surface would produce the observed diffraction pattern, with single-scattering spots the most intense and multiple diffraction spots weaker or absent, depending on the order of multiple scattering. In Fig.5 some first-order hexagonal spots are indicated, one of which lies at $(1+\frac{1}{16}, \frac{3}{5}+\frac{1}{68})$, the other at $(0, \frac{6}{5}+\frac{2}{68})$ in terms of the substrate lattice. By multiple scattering one obtains all other observed extra spots with intensities that are smaller when the reciprocal lattice vectors needed to reach them are longer (long reciprocal lattice vectors produce evanescent waves that contribute less intensity). Relative to bulk bond lengths, this hexagonal layer is contracted by $\frac{1}{26} = 3.85\%$ in one direction, and by 6.47% in the direction perpendicular to that.

Other models besides the hexagonal surface layer model could also reproduce the observed c(26x68) diffraction pattern and we discuss one such model in Section 5 in connection with the shifted-row model for Ir(100).

Pt(100)

Figure 3 shows some of the observed diffraction patterns of reconstructed Pt(100), assuming single domains. Here, as with Au(100) c(26x68), the

absence of many spots can be interpreted as large domains containing many identical (1x5) units. In this case the two different intense parts of any split diffraction spot appear to have almost identical energy dependences so that a domain structure of (1x5) units is a possibility. However, a suitable hexagonal model as proposed by Palmberg[22] for the $\begin{pmatrix} 14 & 1 \\ -1 & 5 \end{pmatrix}$ reconstruction, can also explain the observed pattern. Figure 3 shows this interpretation by inclusion of first-order hexagonal diffraction spots; all other extra spots follow in a manner similar to Au(100) discussed above, by multiple diffraction, the observed spots being obtained by relatively short reciprocal lattice vectors. The above mentioned nearly identical energy dependences of split spots are then a result of the near-symmetry of the pattern.

In the $\begin{pmatrix} 14 & 1 \\ -1 & 5 \end{pmatrix}$ case, cf. Fig.6, one thus obtains a hexagonal layer that is contracted by about 3.5% (nearly isotropically) and rotated by about 0.7° with respect to perfect alignment with the substrate; for the other unit cells shown in Fig.3, hexagonal layers with slightly different contractions and torsions by about 2° are required.

Here also, other models can reproduce the observed diffraction pattern but the particular absence of many spots puts limitations on the possible models. Laser simulation is an effective method of studying such effects since a suitable general theory of two-dimensional diffraction patterns is not available to accurately specify those limitations.

Au(111)

Because of its close relationship with the metal surface reconstructions that are the main topic of this work, the Au(111) reconstruction[11,27,28] deserves special attention. No structural model for this surface has been published to our

knowledge. The observed diffraction pattern is shown in Fig.7. It can be interpreted as the superposition of three 120° rotated domains, each domain consisting of rectangular ($\sqrt{3}$x22) unit cells which we designate ($\sqrt{3}$x22)rect for convenience.

A model consisting of a 4.55% uniaxially contracted hexagonal top layer, cf. Fig.8, satisfies the observed diffraction pattern in terms of single and double diffraction, the contraction direction being a [110] direction. Interestingly, a transmission electron microscope study of Au(111) layer growth in ultrahigh vacuum observed "fringes" (not seen with other metals in (111) orientation) of about 63Å periodicity with just the characteristics expected from the model just described; three 120° rotated domains of the correct orientation. The 63Å periodicity corresponds to about a rectangular ($\sqrt{3}$x22) unit cell and a 4.57% uniaxial contraction. This model appears to be also consistent with recent HEIS results.[28]

A domain-structure model can also be proposed for this reconstruction, involving alternate strips 11 atoms wide of different bulk structure terminations. An interesting possibility is that half the strips have the normal fcc termination, while in the other strips an hcp termination occurs through slippage of the topmost layer to different hollow sites of the second layer. For this model to be stable the two types of termination should have only a small difference in surface energies.

Another possibility for this reconstruction is a charge density wave with an unusually long wavelength of about 22 lattice constants.

5. Surface Structural Models

In any LEED analysis, one must postulate plausible surface structural models and test each against experiment. In this section we discuss plausible models for the Ir, Pt and Au(100) reconstructions.

The hexagonal model

The most popular model for the Ir, Pt and Au(100) reconstructions assumes that the topmost atomic layer takes a hexagonal close-packed arrangement over the square-net substrate[21], cf.Fig.6. There are three main reasons for this idea. First, the hexagonal (111) face of face-centered cubic materials (the three metals studied here have an fcc bulk structure) is known to have the lowest surface energy among the possible crystal faces and it is the closest-packed.[42,43] Therefore, a close packed reconstruction of the (100) face may conceivably lower its surface energy despite the resulting mismatch between the hexagonal layer and the substrate that would increase the strain energy at the surface. Because of the balance of these different surface forces, reconstruction would then happen only for certain metals under certain conditions of cleanliness and temperature. Second, a number of epitaxially grown metallic layers have a crystallographic orientation that corresponds to the building up of hexagonally close packed layers on the substrate surface often independently of the substrate orientation.[44] Thus such a structure appears to have some thermodynamic advantage over others. Third, the reconstruction unit cell of approximately (1x5) dimensions strongly suggest a hexagonal top layer. This was first apparent[21] with Au(100) where the diffraction pattern is such that spots corresponding to a hexagonal layer were clearly identified together with weaker multiple-scattering spots due to combinations of the substrate and hexagonal reciprocal lattices. Furthermore, it is easy to recognize that such a layer, in order to match the substrate mesh exactly, need only contract in one direction (the direction of 5-fold periodicity) by 3.9% with respect to its bulk size; this implies a bond length reduction of only 2.9%. This reduction of bond length is further minimized if one allows the hexagonal layer to buckle, which it surely must do since different top layer atoms must have different

registries and therefore different heights (d-spacings) with respect to the underlying square-net substrate. Thus if one assumes backbond lengths (bond lengths between the top layer and the next layer) equal to the bulk value, the bond lengths parallel to the surface need be contracted by only 0.7 to 1.0%, depending on the registry of the hexagonal layer as a whole. Such contractions seem quite reasonable since analogous contractions have been observed to have values of 1 to 4% for other metal surfaces, namely for backbond lengths on fcc (110), fcc (311), bcc (100) and bcc (111) surfaces.[45]

How much buckling occurs is an important question. An absence of buckling implies the flattest surface (minimum surface area), but maximum buckling (as described above) provides the most constant and bulklike backbond lengths. Surface flatness and constancy of bond lengths are both energetically favorable and so a compromise between the two may be best.

Another interesting question concerns the registry of the hexagonal layer with respect to the substrate. Figure 9 shows the two high-symmetry possibilities. The first involves bridge sites for 2/5 of the atoms we call "two-bridge registry", while the other has 1/5 of the atoms in top sites and 1/5 in center sites which we call "top/center registry". The remaining atoms have less symmetrical sites. Clearly the amount of buckling could depend on the registry. Assuming bulk bond lengths between the top and next layers, the buckling in the top/center registry is ~ 0.8Å, that is $\pm$ 0.4Å deviations about the middle plane, while for the two-bridge registry it reduces to ~ 0.5Å (± 0.25Å deviations). Thus the two-bridge registry provides for a smoother surface. In addition, it gives a more even distribution of the number of nearest neighbors than the top/center registry, that is a more constant coordination number between each surface atom and its neighbors, thereby more evenly spreading the mismatch

among the atoms.

The differences between the LEED patterns of Ir, Pt and Au(100) can be explained conveniently with the hexagonal reconstruction model if one allows the top layer to contract slightly by different amounts, in both directions parallel to the surface, and/or to rotate about the surface normal. A hexagonal layer and a square layer, because of the inherent misfit between a hexagon and a square which essentially provides a slip fault, should have relatively little difficulty in translating or rotating with respect to each other. There is experimental[46] and theoretical evidence[47] for such rotation in Ar overlayers on the basal plane of graphite.

Thus the LEED patterns can be explained by hexagonal reconstructions such as those shown in Fig.6. Ir(100)(1x5) has the simplest structure, a uniaxially contracted hexagonal layer aligned with the substrate orientation (no rotation) as described above. The Pt(100) $\begin{pmatrix} 14 & 1 \\ -1 & 5 \end{pmatrix}$ structure can be explained by a slightly rotated ($\sim$0.7°), biaxially contracted ($\sim$3.55%, not allowing for buckling) hexagonal layer with a coincidence lattice spanned by the vectors (14,1)a and ($\bar{1}$,5)a (a being the substrate square edge). A very slight distortion by an angle of about 2° of this layer produces the observed $\begin{pmatrix} 14 & 1 \\ 0 & 5 \end{pmatrix}$ structure spanned by the vectors (14,1)a and (0,5)a. Other contractions and distortions and/or rotations can produce the other observed structures.

Instead of a simple rigid rotation of the hexagonal layer as discussed above, one may also imagine an unrotated (1x5) hexagonal structure to have dislocations every 14 atomic rows apart[24], producing a $\begin{pmatrix} 14 & 1 \\ -1 & 5 \end{pmatrix}$ or similar superstructure. The dislocation need not be abrupt, it may be spread out over several atomic rows. An abrupt dislocation would be rather jagged and thus energetically unfavorable unless a $\begin{pmatrix} 14 & 1 \\ -3 & 5 \end{pmatrix}$ structure were adopted. This is

shown in Fig. 10. The dislocations follow the rows of atoms, avoiding any jaggedness. A spread-out rather than abrupt dislocation as illustrated in Figure 10 is also consistent with the $\begin{pmatrix} 14 & 1 \\ -1 & 5 \end{pmatrix}$ and $\begin{pmatrix} 14 & 1 \\ 0 & 5 \end{pmatrix}$ geometries. Such a spread-out dislocation can also be regarded as just a relaxation of the rotated hexagonal models if one allows atoms to have preferences for some adsorption sites over others, thereby letting atoms move as much as they can toward the nearest preferred sites.

Finally, the Au(100) c(26x68) surface would have a hexagonal layer without rotation but with 3.85% and 6.47% contractions in the 26-fold and 68-fold periodicity directions, respectively, corresponding to the 20-fold and 5-fold directions, respectively, in the (20x5) notation.

It is intriguing to compare the (1x5) hexagonal model discussed here with a recently discovered (1x5) reconstruction of the clean V(100) surface.[4] Vanadium has a bcc lattice and it so happens that a planar (110) layer, the closest packed of the bcc layers, can fit on the square-net (100) substrate with a (1x5) superlattice if a 3% contraction or an appropriate buckling in the 5-fold direction is allowed; 8 top layer atoms then fit in the (1x5) unit cell.

A difficulty with the hexagonal model is the 20% higher concentration of atoms in the topmost layer of such a reconstructed surface as compared with the unreconstructed (1x1) surface: about 6 rows of atoms in a hexagonal layer fit over five rows of atoms of the square substrate. The transition between the unreconstucted and reconstructed states occurs experimentally quite easily. Where do the 20% more atoms come from? Apart from the presumably insufficient number of defect atoms (metal adatoms migrating along the surface), the always present steps in the surface can provide the answer. A terrace bound by a step may contract parallel to the surface with the step retreating over the terrace

Of course.
below it ./ all successive steps would retreat in this way by similar amounts leaving the step-to-step distance constant, but each retreating step exposes formerly unexposed second-layer atoms which provide the additional 20% surface atoms. Because the terraces should be at least a few hundred Angstroms wide to give the observed sharp LEED patterns, the step edges would then have to retreat by at least several tens of Angstroms in a reconstruction.

The missing row hexagonal model

To avoid the problem of 20% higher surface concentration in the hexagonal model one may imagine that the hexagonal model is formed in strips five atoms wide with one vacancy row between such strips. We may call this the missing row hexagonal model. The formation of such a surface, however, would increase the surface energy. In considering this model in our analysis, we assume that the missing rows are in symmetry planes, such as the row of top-site atoms for the top/center registry, or a row of bridge-site atoms for the two / bridge registry. This way we keep high symmetry in the surface structure.

To produce the Pt(100) and Au(100) structures one would have to imagine a suitable domain structure to match the large observed unit cells. However, it is not clear what physical mechanism could produce the necessary ordering of missing rows.

The shifted row models

Another set of (1x5) structures which do not require a 20% higher surface concentration we call shifted row models. This type of model was originally proposed by Burton and Jura.[48] Here two of the five atoms in each (1x5) unit cell are shifted[49] as indicated in Fig.11; depending on the choice of shift,

three basic structures are possible. One obtains a greater degree of close-packing than in the unreconstructed surface at the price of opening up channels with broken bonds. Compared with the hexagonal model, the shifted row models have less misfit between the top layer and the substrate, but more misfit within the top layer. An advantage over the hexagonal model is that no bond length contraction is needed and that less movement of atoms is required in the reconstruction process. Also, this model provides an explanation for the decrease of the work function upon transition from an unreconstructed to a reconstructed Ir(100) surface. The work function decreases since the roughness of the surface increases. One expects a higher work function with a (111)-type top layer in analogy with the unreconstructed (111) face, neglecting effects due to the hexagon-square interface. There is no fundamental preference in this model for the observed 5-fold periodicity. Other periodicities could occur as well. A 7-fold periodicity has been observed in one experiment[43a] supporting the plausibility of this model; this occurs when three or four layers of gold are deposited on a (100) surface of palladium (although here the lattice constant of the gold substrate may be affected by the palladium substrate below the gold). Also, streaks have been observed in [110] directions when gold is deposited in certain coverages on Pt(100), indicating a disorder in the 5-fold period.[50]

One of the main arguments against the model proposed originally by Burton and Jura is that the atoms of the shifted rows are in bridge sites and, therefore, probably in an unstable situation. Surface phonon calculations have been carried out in the case of a (2x1) reconstruction involving a shift of every other row, showing that there is indeed an instability for low frequency phonons in this configuration.[51] Figure 11 shows that in fact the model proposed here is slightly different since here each atom of the shifted rows is moved to the

3-fold site formed by two of the unshifted atoms and one atom of the second layer.

To explain the Pt(100) and Au(100) reconstructions, regularly spaced defects have to be introduced in the shifted rows model. Figure 12 shows a sketch of a possible model associated with the reconstruction of platinum. Here the shifted atoms form rows of a finite length (14 atoms long) instead of the infinite length rows of iridium. Similar dislocations can also produce the various other observed unit cells.

The length of 14 for the shifted rows could be explained by a contraction or expansion of the atomic size by a factor 1/14; then each shifted row would contain 15 or 13 atoms, respectively. This would permit a smooth transition at the ends of each shifted row. It would also remove the criticism raised for Au(100) that all split parts of a spot should have a similar energy dependence since we no longer have a simple domain structure.

A suitable model for the Au(100)c(26x68) reconstruction involves dislocations in two directions instead of one for platinum. Figure 12 shows a sketch of a possible structure. In one of the directions the type of defect is similar to that of platinum (finite chains of 14 shifted atoms), but platinum shows no defects in the other direction. For Au(100) there is a different interaction between chains and there appears a stacking fault of chains after every 34 chains. In Fig. 12 we have represented the models with three unshifted rows followed by two shifted ones, corresponding to Fig. 11c. A similar model can be built with the structures shown in Figues 11d and 11e.

This model for Au(100) explains the difference in the nature of the spot splittings. One one hand, the doublet formation many authors have observed and which gives rise to the designation (20x5) is associated with the first type of defect (finite length of shifted rows), while the V-shaped triplet formation

which few experiments show[27,28] is associated with the second type of defect , such as interaction between chains. This second type requires a much better ordering of the surface since first the chains have to be formed and then ordered.

Such dislocations are very common in three dimensions with polytype crystals, and it would not be surprising of a similar effect could exist at surfaces. In the preceding section we proposed a model of this type for the Au(111) reconstruction as well.

An argument against the shifted row models is the HEIS observation that about one full monolayer is shifted out of alignment with chains of substrate atoms for Pt(100), Au(100), and Au(111).

The charge-density wave (CDW) model.

Several clean surface reconstructions have been described as charge density waves (CDW's), including W(100)c(2x2)[17] for which a LEED analysis gives a structure consistent with a CDW, Mo(100),[17] Si(111)(7x7),[18] and 1T-TaS_2(0001)[19] with various superstructures, among them $(\sqrt{13}x\sqrt{13})$. In a CDW[51] atoms are displaced from their ideal position in a wavelike pattern by no more than about 0.1Å. A (1x5) structure on fcc(100) can be obtained with a CDW that has a wavelength 5a (a=bulk bond length) and direction parallel to rows of close-packed atoms, such as [011]. The $\begin{pmatrix} 14 & 1 \\ -1 & 5 \end{pmatrix}$c(26x68) and similar structures can be obtained with pairs of CDW's of different wavevectors. The Au(111) structure can also be interpreted as a long wavelength CDW.

Many other surface models in addition to those discussed here can be imagined which will fit the (1x5) and other observed unit cells (missing rows, additional rows above the surface, etc.) but none that we considered seemed intuitively more plausible than the models described above.

6. Laser simulation

Laser simulation of LEED patterns has been frequently used in the past

to test various types of surface structure models, especially when large unit cells, domain structures, or disorder are involved. The basis of this technique is described by Ellis.[53] Fedak, et al.[54] have applied this technique to the reconstruction of Au(100), supporting their conclusion of a hexagonal top-layer model with some modulation. Laser diffraction was also used in a recent study of the Pt(100) reconstruction.[25] We have used this approach to study many more models for these reconstructions than has been done previously.

Our implementation of laser simulation is quite simple. The surface atoms are represented by arrays of dots (usually small dots for the first substrate layer and large dots for the top layer), computer drawn directly onto microfiche or 35 mm film with a basic lattice constant of typically 30 μm. This produces convenient diffraction spot separations on a screen a few meters away and an overall size comparable to the laser beam diameter of about 1 mm. Since the coherence length across the laser beam is about equal to its diameter, we effectively simulate a LEED beam coherence length of about 100Å, a realistic result. For simplicity we have not attempted to include different domain orientations simultaneously since one domain orientation is sufficient for the purposes of the following discussion. Atomic displacements perpendicular to the surface (such as in a layer buckling) are simulated by dot displacements of proportional magnitude parallel to the plane of the film.

We now consider what laser diffraction can teach us concerning the surface models proposed in Section 5 in relation to the observed LEED patterns for the reconstructed Ir, Pt and Au(100) surfaces. For convenience, we shall term the integral-order spots (those present without reconstruction) substrate spots, while those due to a hexagonal array by itself are called hexagonal spots, even though the hexagon may be somewhat distorted.

Ir(100)

Starting with the simple nonbuckled (1x5) structure of the hexagonal model (cf. Figs. 6 and 9), we find that only the substrate and hexagonal spots have strong intensity in laser diffraction, as seen in Fig.13c. To obtain an intensity in the other extra spots comparable to the intensity of the substrate and hexagonal spots, as required by the experimental observation for Ir, it is necessary to include a modulation of the top-layer atomic positions in the 5-fold direction. This suggests that the real Ir(100)(1x5) surface also has such a modulation. The obvious choice is a buckling perpendicular to the surface already described in Section 5. Laser simulation leads to the same conclusion for the Pt and Au structures based on the hexagonal model; a buckling is also likely there. Note that with such buckling the extra spots are already present in the kinematic limit; multiple scattering is not required to produce them.

We find that laser diffraction puts few limitations on the missing row and shifted rows models for the (1x5) structure. Some typical patterns are shown in Figs. 13b and 13c. However, the charge-density-wave model does not produce adequate intensity in the extra spots, cf. Fig.13e.

Pt(100) and Au(100)

Concerning the $\begin{pmatrix} 14 & 1 \\ -1 & 5 \end{pmatrix}$,c(26x68) and similar surface structures, the simple hexagonal model produces realistic laser diffraction patterns, but it is necessary, in order to obtain sufficient intensity in the split spots away from the (1x5) spot positions, to include a modulation of atomic positions in the 14-fold and 26-fold directions, respectively. This comes in addition to the modulation needed in the 5-fold direction. The effect is seen in Figs. 13g and 13h. As above, this may be indicative of buckling. Buckling would be reasonable in

in this direction as well, since different atoms would have different registries as a result of the contraction of the layer by factors of 1/14 and 1/26, respectively. Sufficient intensity in the split spots for Pt(100) may also be obtained by the spread-out dislocation model of Fig. 10, which includes not only a possible buckling, but also a position modulation parallel to the surface. It is interesting to observe what happens as the dislocation becomes more localized; more and more spots appear which extend from one row of 1/5th order spot positions to the next, cf. Fig.13. If the dislocation were of the domain boundary type, all these additional spots would disappear again. Thus patterns very similar to those of Figs. 13g and 13h could also be produced (not shown) with the dislocation model of the shifted rows structure (Fig.12).

The Au(100)c(26x68) unit cell is so large that it was not possible to perform the laser diffraciton satisfactorily in this case. However, by approximating the structure with a (20x5) unit cell, we obtain with the hexagonal model the same effects due to position modulations as with the Ir and Pt structures shown in Figs.13j and 13k. The V shape of diffraction multiplets observed in LEED could also be produced (not shown) with suitably reduced unit cells. This is possible with both the hexagonal and the shifted-rows models.

Au(111)

In Fig.13' we show a laser diffraction pattern for Au(111) ($\sqrt{3}$x22) rect , modeled in Fig.8, without position modulations. Inclusion of such modulations would multiply the number of split-off spots, reproducing the appearance of Fig.7. A charge-density-wave structure for Au(111) ($\sqrt{3}$x22) rect would also be capable of producing the observed diffraction pattern, especially if a few higher harmonics of the basic periodicity are included.

Conclusions

We reach the following conclusions based on laser simulation. The hexagonal model is realistic and probably requires buckling or a similar position

modulation. The missing row and shifted rows models are also compatible with the LEED patterns. However, no abrupt dislocations other than domain boundaries should occur as one moves in the direction perpendicular to the 5-fold direction. Also the charge-density-wave model can be ruled out for the (100) reconstructions.

7. Summary

In this paper we have brought together and analyzed the various observed reconstructions of the Ir(100), Pt(100), Au(100) and Au(111) surfaces. Ir(100) shows a simple (1x5) structure (no spot splittings) indicating a relatively small unit cell. Pt (100) exhibits a variety of patterns, including $\begin{pmatrix} 14 & 1 \\ -1 & 5 \end{pmatrix}$, $\begin{pmatrix} 14 & 1 \\ 0 & 5 \end{pmatrix}$, $\begin{pmatrix} 12 & 1 \\ -3 & 5 \end{pmatrix}$ and $\begin{pmatrix} 27 & 2 \\ -3 & 6 \end{pmatrix}$, some of which occur on stepped Pt(100) surfaces. According to high quality diffraction patterns Au(100) has a c(26x68) reconstruction which, in lower quality patterns, appears approximately as a (20x5) structure. On stepped Au(100) surfaces a $\begin{pmatrix} 14 & 1 \\ -1 & 5 \end{pmatrix}$ structure has also been observed. Au(111) reconstructs with a rectangular $(\sqrt{3}\times 22)$ unit cell.

This paper also describes the measurement of LEED intensities for Ir(100) and Pt(100). These are to be used in a detailed structural analysis with dynamical calculations (see following paper); but first we interpret the LEED patterns in terms of possible structural models and do a laser simulation to test those models and some of their parameters. The hexagonal top-layer model can explain all observed diffraction patterns with varying contractions and rotations of the top layer. The laser simulation indicates that this model probably requires a buckling perpendicular to the surface. The missing row hexagonal model and the shifted row models cannot be ruled out by laser diffraction, but have to include suitable domain structures to explain the more complicated LEED patterns. Models based on charge density waves can be ruled out, however, for the (100) faces.

Acknowledgements

We are thankful to Drs. D.M. Zehner and J.F. Wendelken for kindly providing us with photographs of Au(100) and (111) diffraction patterns.

This work was supported by the Division of Materials Sciences, Office of Basic Energy Sciences, U.S. Department of Energy.

Prepared for the U.S. Department of Energy under contract W-7405-ENG-48.

References

1. J.T. Grant, Surface Sci. 18 (1969) 228.
2. S. Hagstrom, H.B. Lyon and G.A. Somorjai, Phys. Rev. Lett 15 (1965) 491.
3. D.G. Fedak and N.A. Gjostein, Phys. Rev. Lett. 16 (1966) 171.
4. P.W. Davies and R.M. Lambert, subm. to Surface Sci.
5. G. Gewinner, J.C. Peruchetti, A. Jaegle and R. Riedinger, Phys. Rev. Lett. 43 (1979) 935.
6. T.E. Felter, R.A. Barker and P.J. Estrup, Phys. Rev. Lett. 38 (1977) 1138.
7. K. Yonehara and L.D. Schmidt, Surface Sci. 25 (1971) 238.
8. K. Christmann and G. Ertl. Z. Naturforsch. 28a (1973) 1144.
9. H.P. Bonzel and R. Ku, Surface Sci. 33 (1972) 91.
10. D.G. Fedak and N.A. Gjostein, Acta Met. 15 (1967) 827.
11. J. Perdereau, J.P. Biberian and G.E. Rhead, J. Phys. F 4 (1974) 798.
12. P.J. Estrup and J. Anderson, J. Chem Phys. 45 (1966) 2254.
13a. C.A. Haque and H.E. Farnsworth, Surface Sci. 1 (1964) 378.
13b. J.E. Demuth, J. of Colloid and Interface Sci. 58 (1977) 184.
14. R.A. Barker, P.J. Estrup, F. Jona and P.M. Marcus, Sol. St. Comm. 25 (1978) 375.
15. C.-M. Chan, M.A. Van Hove, W.H. Weinberg and E.D. Williams, Sol. St. Comm 30 (1979) 47; Surface Sci.
16. W. Moritz and D. Wolf, Surface Sci. 88 (1979) L29.
17a. J.E. Inglesfield, J. Phys. C11 (1978) L69.
17b. E. Tosatti, Sol. St. Comm. 25 (1978) 637.
18. E. Tosatti and P.W. Anderson, Jpn. J. Appl. Phys. Suppl. 2, Pt.2 (1974) 381.
19. B.J. Mrstik, R. Kaplan, T.L. Reinecke, M. Van Hove and S.Y. Tong, Il Nuovo Cimento 38B (1977) 387; the notation 1T specifies a particular layer stacking of this layer compound.
20. A.M. Mattera, R.M. Goodman and G.A. Somorjai, Surface Sci 7 (1967) 26.
21. D.G. Fedak and N.A. Gjostein, Surface Sci. 8 (1967) 77.
22. P.W. Palmberg, in The Structure and Chemistry of Solid Surfaces, ed. G.A. Somorjai, John Wiley & Sons, Inc, New York, 1969, p. 29-1.
23. P.C. Stair, Ph.D. Thesis, University of California, Berkeley, 1976.
24. D.W. Blakely, Ph.D. Thesis, University of California, Berkeley, 1976.
25. K. Heinz, P. Heilmann and K. Müller, Z. Naturforsch. 32a (1977) 28.

26. P.R. Norton, private communication.

27. J.F. Wendelken and D.M. Zehner, Surface Sci. 71 (1979) 178.

28. D.M. Zehner, private communication.

29. H. Melle and E. Menzel, Z. Naturforsch. 33a (1978) 282.

30. P.R. Norton, J.A. Davies, D.P. Jackson and N. Matsunami, Surface Sci. 85 (1979) 269.

31. D.M. Zehner, B.R. Appleton, T.S. Noggle, J.W. Miller, J.H. Barrett, L.H. Jenkins and O.E. Schow III, J. Vac. Sci. Technol. 12 (1975) 454.

32. J. Küppers and H. Michel, Appl. Surface Sci. 3 (1979) 179.

33. P. Heimann, J. Hermanson, H. Miosga, and H. Neddermeyer, Phys. Rev. Lett. 43 (1979) 1757.

34. E.W. Müller and T.T. Tsong, Field Ion Microscopy, American Elsevier Publ. Co., New York, 1969.

35. A.J. Melmed, R.T. Tung, W.R. Graham and G.D.W. Smith, Phys. Rev. Lett. 43 (1979) 1521.

36. T.N. Rhodin and G. Broden, Surface Sci. 60 (1976) 466.

37. H.P. Bonzel, C.R. Helms and S. Kelemen, Phys. Rev. Lett 35 (1975) 1237.

38. A. Ignatiev, A.V. Jones, and T.N. Rhodin, Surface Sci. 30 (1972) 573.

39. P. Heilmann, K. Heinz and K. Müller, Surface Sci. 83 (1979) 487.

40. R. Feder, Surface Sci. 68 (1977) 229.

41. K. Tagi, K. Takayanagi, K. Kobayashi, N. Osakabe, Y. Tanishiro and G. Honjo, Proc. 9th Intern'l. Congr. on Electron Microscopy, Toronto, 1978, J.M. Sturgess, ed., Vol. I, p. 458.

42a. W.L. Winterbottom, in Surfaces and Interfaces, J.J. Burke et al., eds. Syracuse Univ. Press, Syracuse, New York, 1967.

42b. C. Herring, in Structure and Properties of Solid Surfaces, R. Gomer and C.S. Smith, eds. Univ. of Chicago Press, Chicago, 1962.

43. T.N. Rhodin, P.W. Palmberg and E.W. Plummer, in Structure and Chemistry of Solid Surfaces, Ed. G.A. Somorjai, John Wiley & Son, Inc., New York, 1969.

44. see, for example: a) P.W. Palmberg and T.N. Rhodin, J.Chem. Phys. 49 (1972) 134; and b) J. Henrion and G.E. Rhead, Surface Sci. 29 (1972) 20.

45a. M.A. Van Hove and S.Y. Tong, Surface Crystallography by LEED, Springer-Verlag, Heidelberg, 1979.

45b. G.A. Somorjai and M.A. Van Hove, in Adsorbed Monolayers on Solid Surfaces, Structure and Bonding, Vol. 38 (1979) 1.

46. C.G. Shaw, S.C. Fain, Jr., and M.D. Chinn, Phys. Rev. Lett 41 (1978) 955.

47. A.D. Novaco and J.P. McTague, Phys. Rev. Lett. 38 (1977) 1286.

48. J.J. Burton and G. Jura, in Structure and Chemistry of Solid Surfaces, Ed. G. A. Somorjai, Johns Wiley & Son, Inc., New York, 1969.

49. J.P. Biberian, to be published.

50. J.W.A. Sachtler, private communication.

51. C. Annett, W.R. Lawrence and R.E. Allen, Phys. Rev. B10 (1974) 4184.

52. J.A. Wilson, F.J. DiSalvo and S. Mahajan, Adv. in Phys. 24 (1975) 117.

53. W.P. Ellis, in Optical Transforms, H.S. Lipton, ed., Academic Press, New York, 1972.

54. D.G. Fedak, T.E. Fischer and W.D. Robertson, J. Appl. Phys. 39 (1968) 5658.

Figure Captions

Figure 1 LEED patterns for clean reconstructed Ir(100).

Figure 2 LEED patterns for clean reconstructed Pt(100). Four domains are present in (a); only two domains are present in (b).

Figure 3 Unit cells and schematic LEED patterns for different reconstructions of Ir and Pt(100). Dot size is roughly proportional to average spot intensity. Triangular dots represent "hexagonal spots" due to a hexagonal layer.

Figure 4 LEED patterns for clean reconstructed Au(100) (courtesy of J.F. Wendelken and D.M. Zehner).

Figure 5 Schematic LEED pattern for clean reconstructed Au(100), with unit cell in reciprocal space. Conventions as in Figure 3.

Figure 6 Hexagonal models for Ir(100)(1x5) and Pt(100) $\begin{pmatrix} 14 & 1 \\ -1 & 5 \end{pmatrix}$ reconstructions. Top layer atoms are shown as thick circles, next layer as thin circles. The two-bridge registry is assumed.

Figure 7 LEED diffraction patterns for clean reconstructed Au(111) (courtesy of J.F. Wendelken and D.M. Zehner).

Figure 8 Hexagonal model for Au(111) ($\sqrt{3}$x22) rect reconstruction. Conventions as in Figure 6.

Figure 9 Detail of hexagonal model for Ir(100)(1x5) with two registries. Side views, parallel to the surface, are shown at top, exhibiting full buckling. Views from top are shown at bottom. Thick circles represent atoms closer to the viewer than thin circles.

Figure 10 Hexagonal-layer dislocation model for Pt(100) $\begin{pmatrix} 14 & 1 \\ -3 & 5 \end{pmatrix}$ compared to Ir(100)(1x5) model shown in (a); (b) gradual dislocation; (c) abrupt dislocation.

Figure 11 Five models in top view for the reconstruction of Ir(100)(1x5). (a) hexagonal model with two-bridge registry, (b) hexagonal model with center/top registry, (c) shifted rows model with 5-atom clusters, (d) as (c) with 4-atom clusters, and (e) as (c) with 3-atom clusters.

Figure 12 Sketched domain structure of the shifted rows model for Pt(100)

$\begin{pmatrix} 14 & 1 \\ -1 & 5 \end{pmatrix}$ and $\begin{pmatrix} 14 & 0 \\ -1 & 5 \end{pmatrix}$ (left) and for Au(100)c(26x68) (right) assuming 5-atom clusters. Only the top layer is shown. Unshifted rows of atoms are represented by continuous line segments; shifted rows (possibly contracted or expanded) are represented by dashed lines.

Figure 13 Laser diffraction patterns for various models of the (100) reconstructions of Ir (a-f), Pt (g-i), and Au (j,k) and of the (111) reconstruction of Au (only one domain is included in each pattern). Substrate spots are sometimes weak in these patterns.

a,b Ir(100)(1x5) hexagonal model, without (a) and with (b) a position modulation in the 5-fold direction.

c Ir(100)(1x5) hexagonal model with missing rows.

d Ir(100)(1x5) shifted rows model (3-atom clusters).

e,f Ir(100)(1x5) charge density wave model with 0.1 Å and 0.4 Å amplitudes, respectively.

g,h Pt(100) $\begin{pmatrix} 14 & 1 \\ -1 & 5 \end{pmatrix}$ hexagonal model with one (g) or two (h) sine-wave position modulations in the 14-fold direction. A modulation in the 5-fold direction is included in both cases.

i Pt(100) $\begin{pmatrix} 14 & 1 \\ -3 & 5 \end{pmatrix}$ hexagonal model with abrupt dislocations as in Figure 10.

j,k Au(100)(20x5) hexagonal models without (j) and with (k) position modulations in both the 5-fold and 20-fold directions. Pattern (k) is very similar to low resolution LEED patterns.

l Au(111)($\sqrt{3}$x22)rect hexagonal model without position modulation.

IR (100) - 5x1
$\theta = 0, \phi = 0$
T = 300 K

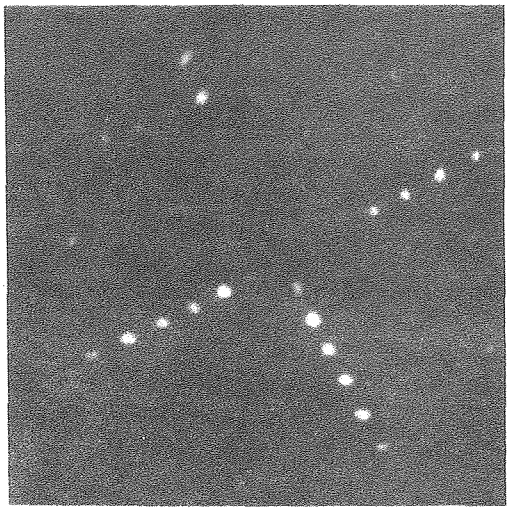

48 eV

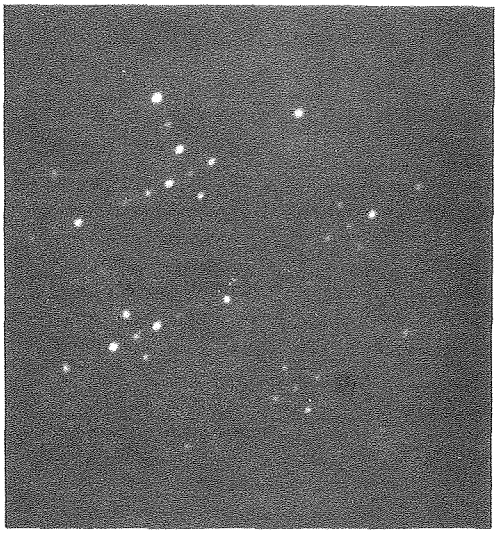

100 eV

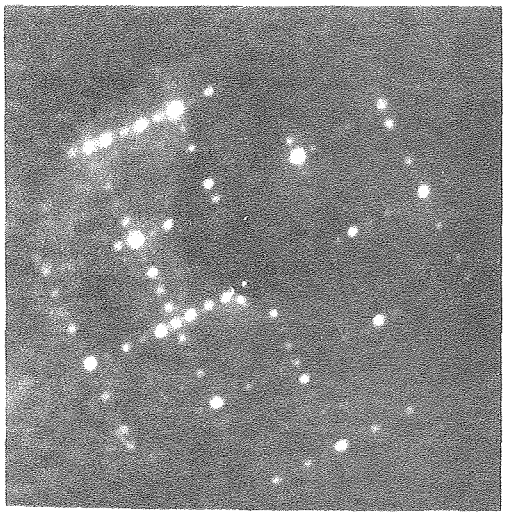

175 eV

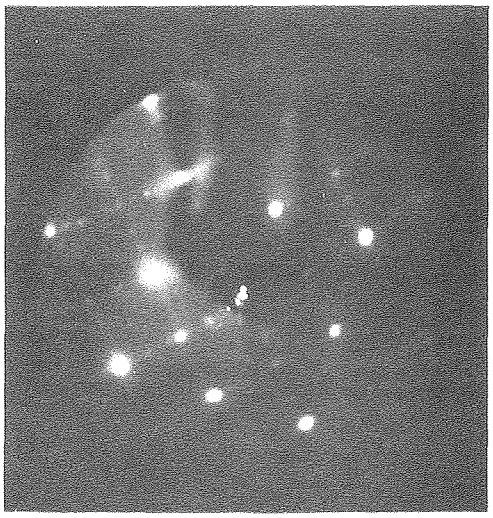

273 eV

Fig.1

XBB 790-16403

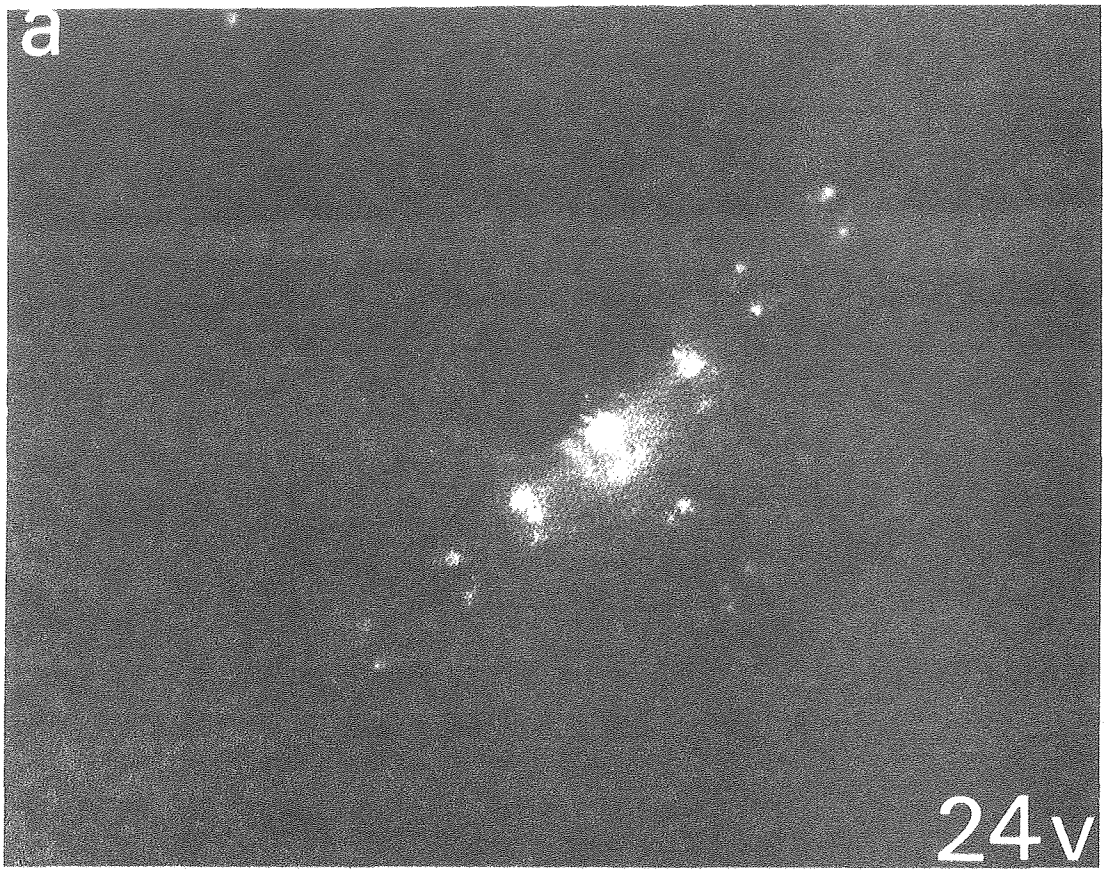

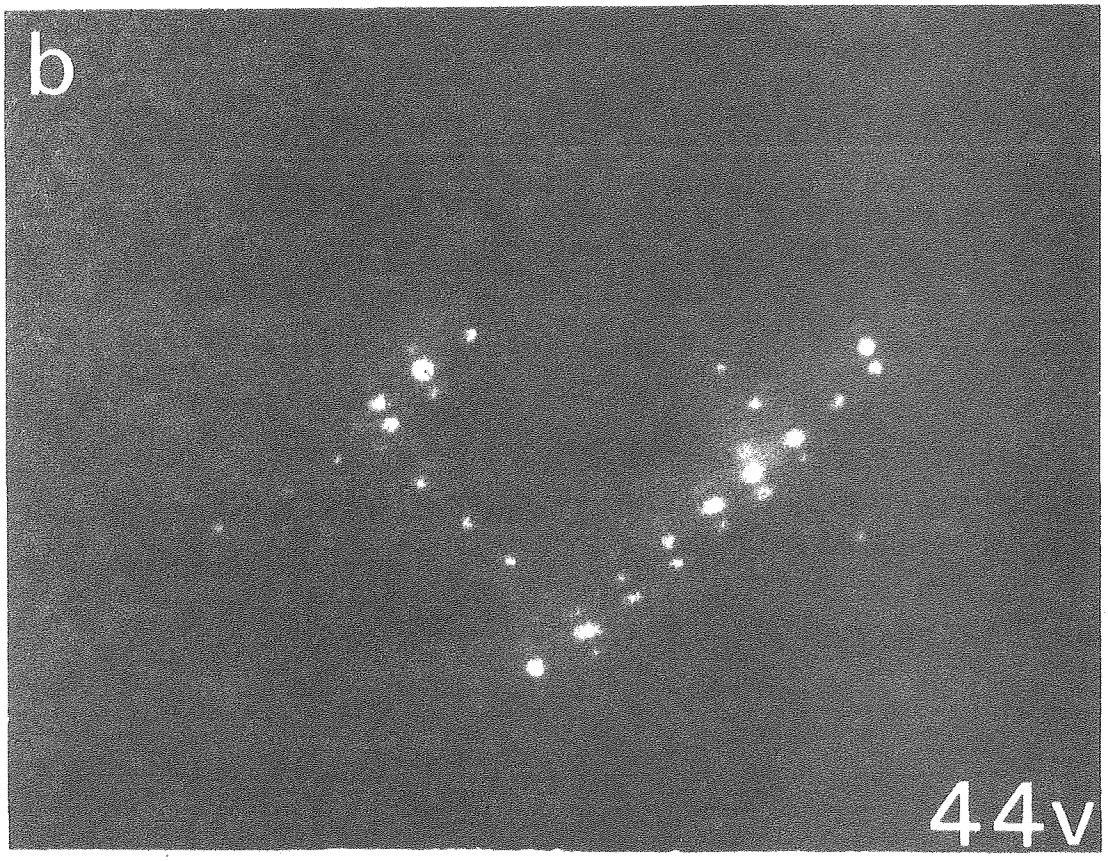

Fig.2

XBB 774-2914

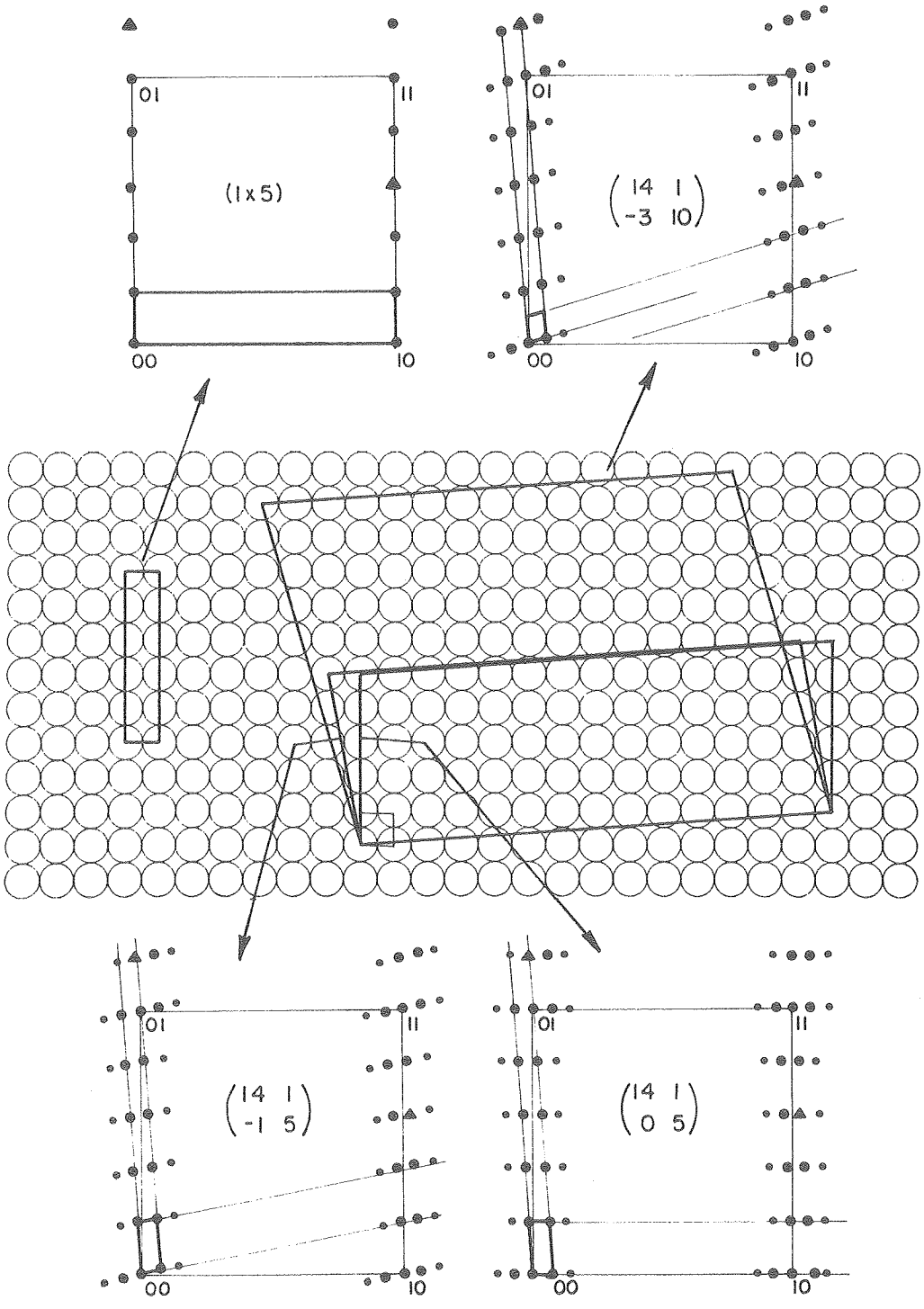

XBL 7911-14542

Fig.3

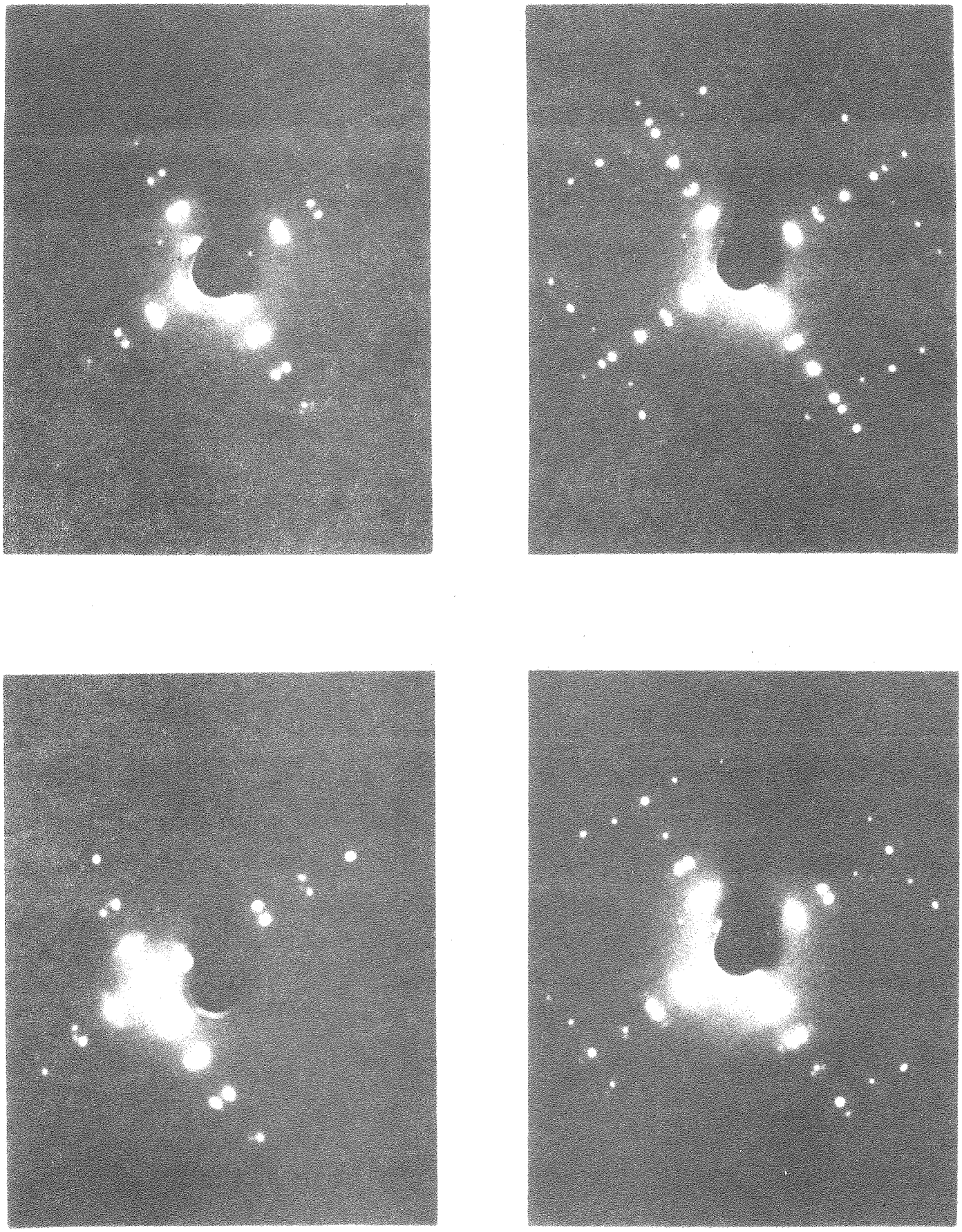

Fig.4

XBB 790-13985

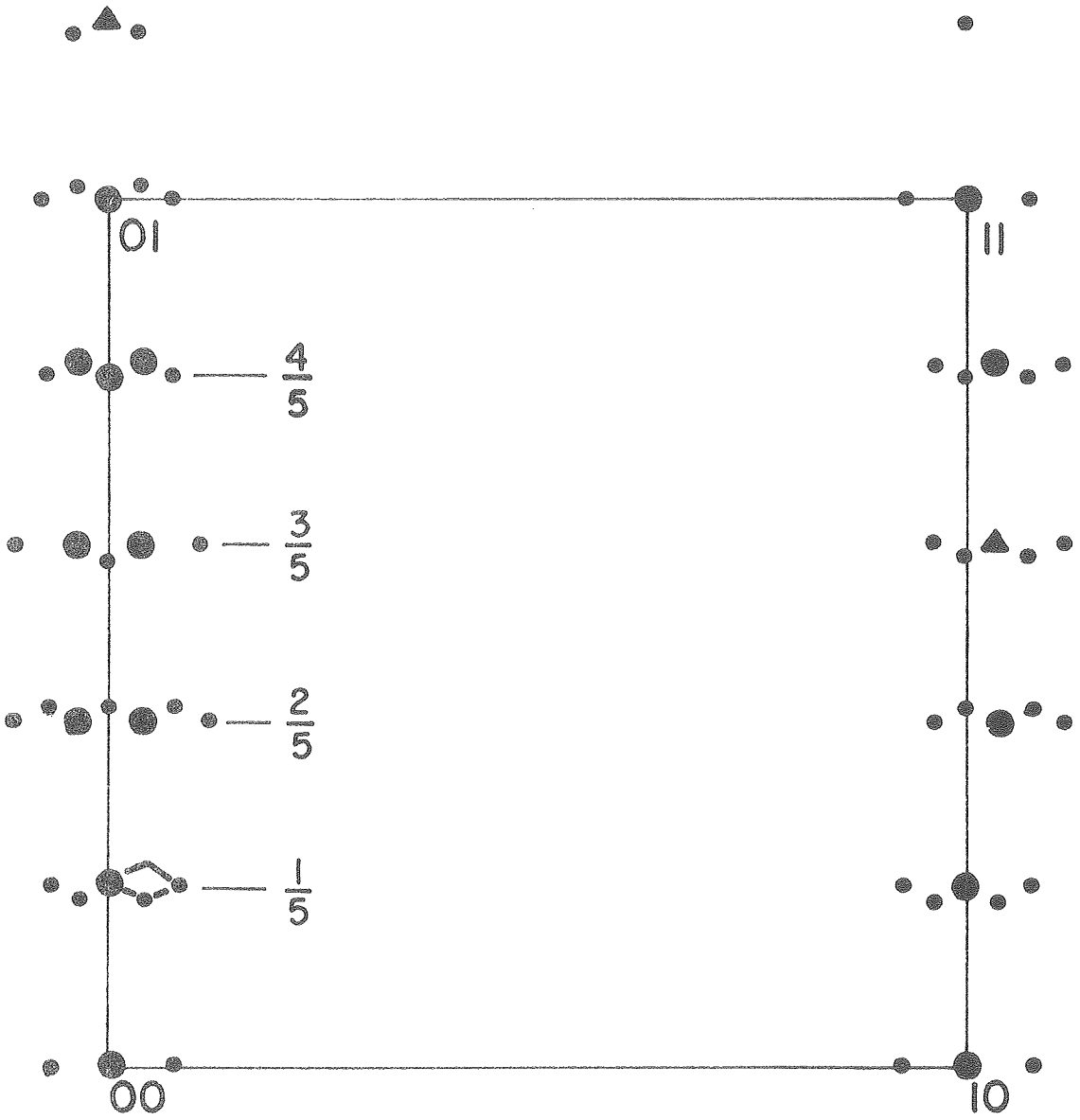

Au (100) c (26×68)

XBL 7911-14543

Fig. 5

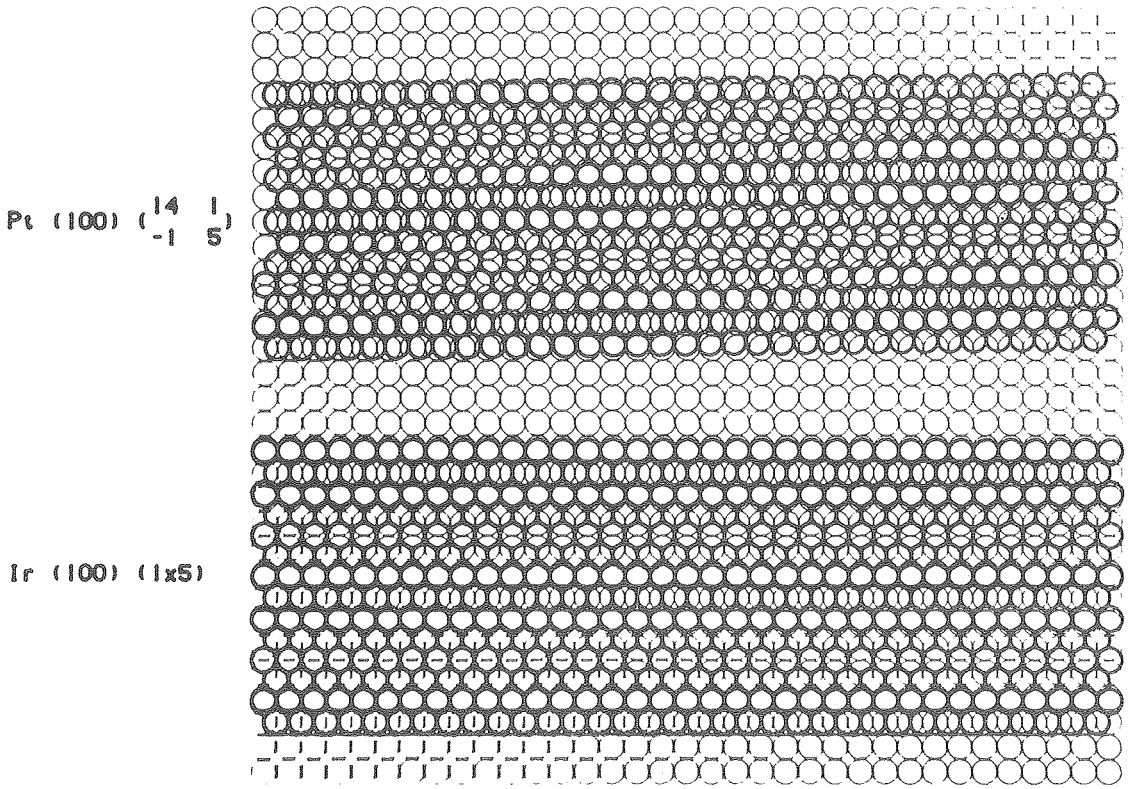

XBL 7912-13736

Fig.6

Au(111)

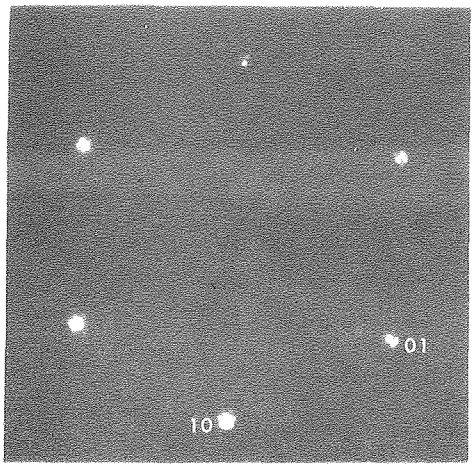

46 V

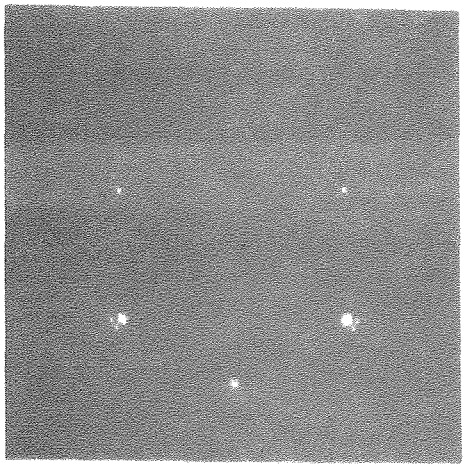

80 V

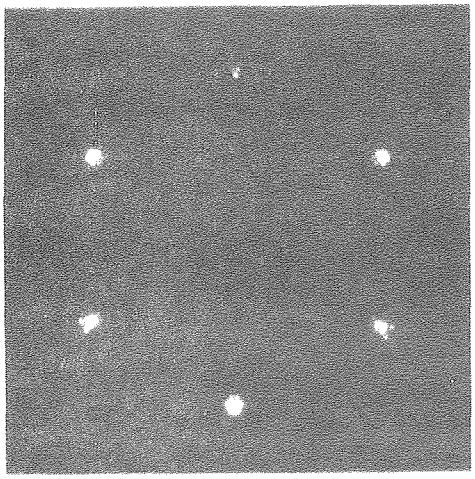

54 V

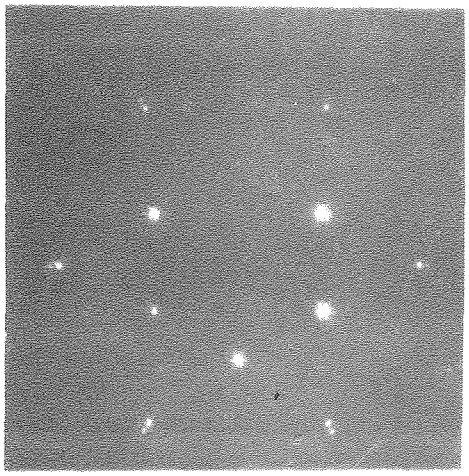

133 V

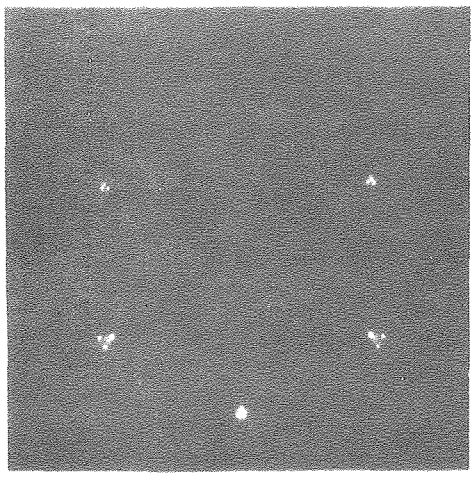

64 V

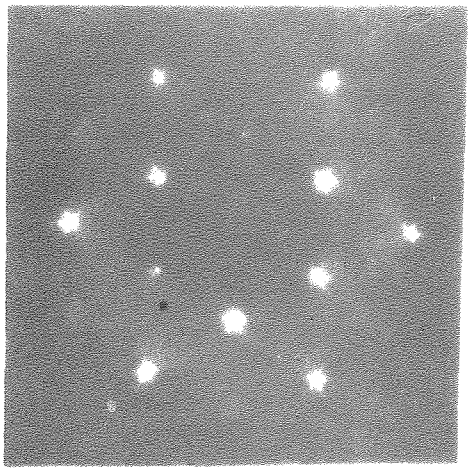

145 V

Fig.7

XBB 790-13988

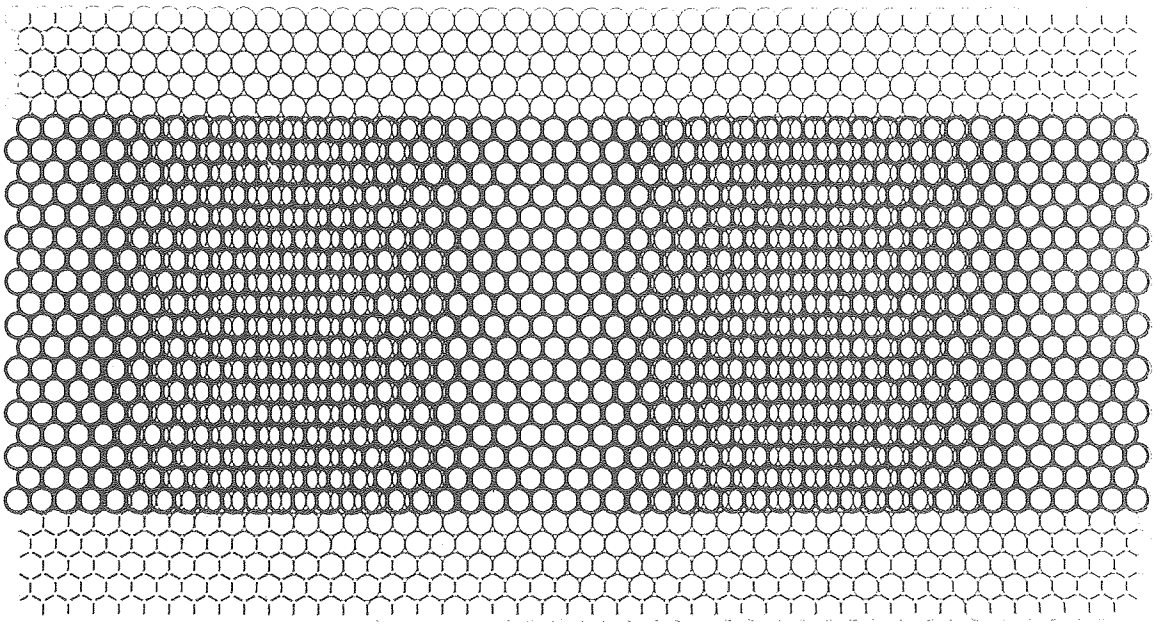

Au (111)(R3x22)rect

XBL 7912-13738

Fig.8

fcc (100) : buckled hexagonal top layer

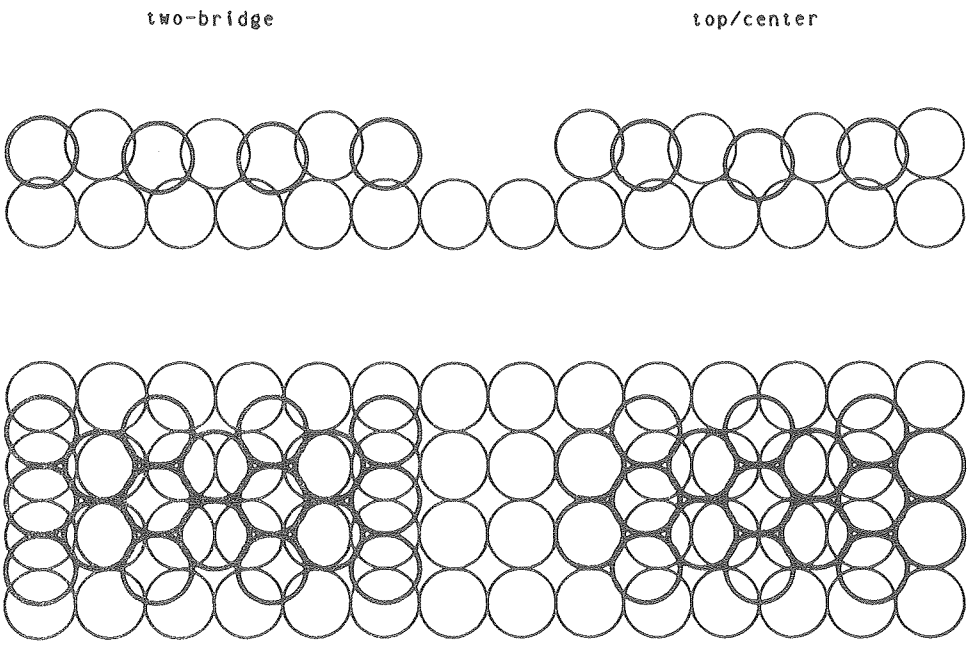

XBL 7912-13739

Fig.9

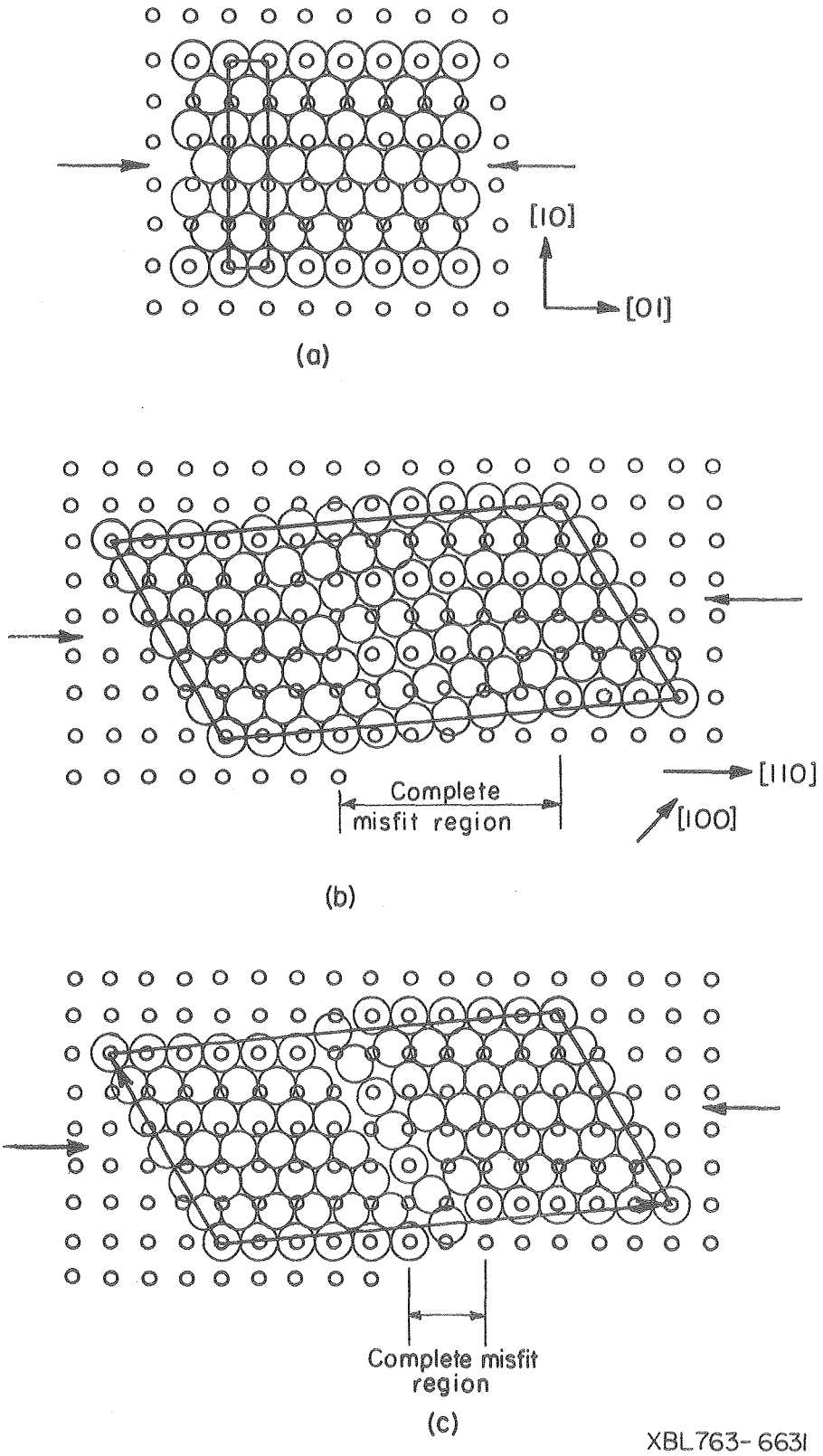
[10]
[01]
(a)
Complete
misfit region
[110]
[100]
(b)
Complete misfit
region
(c)
XBL763-6631

Fig. 10

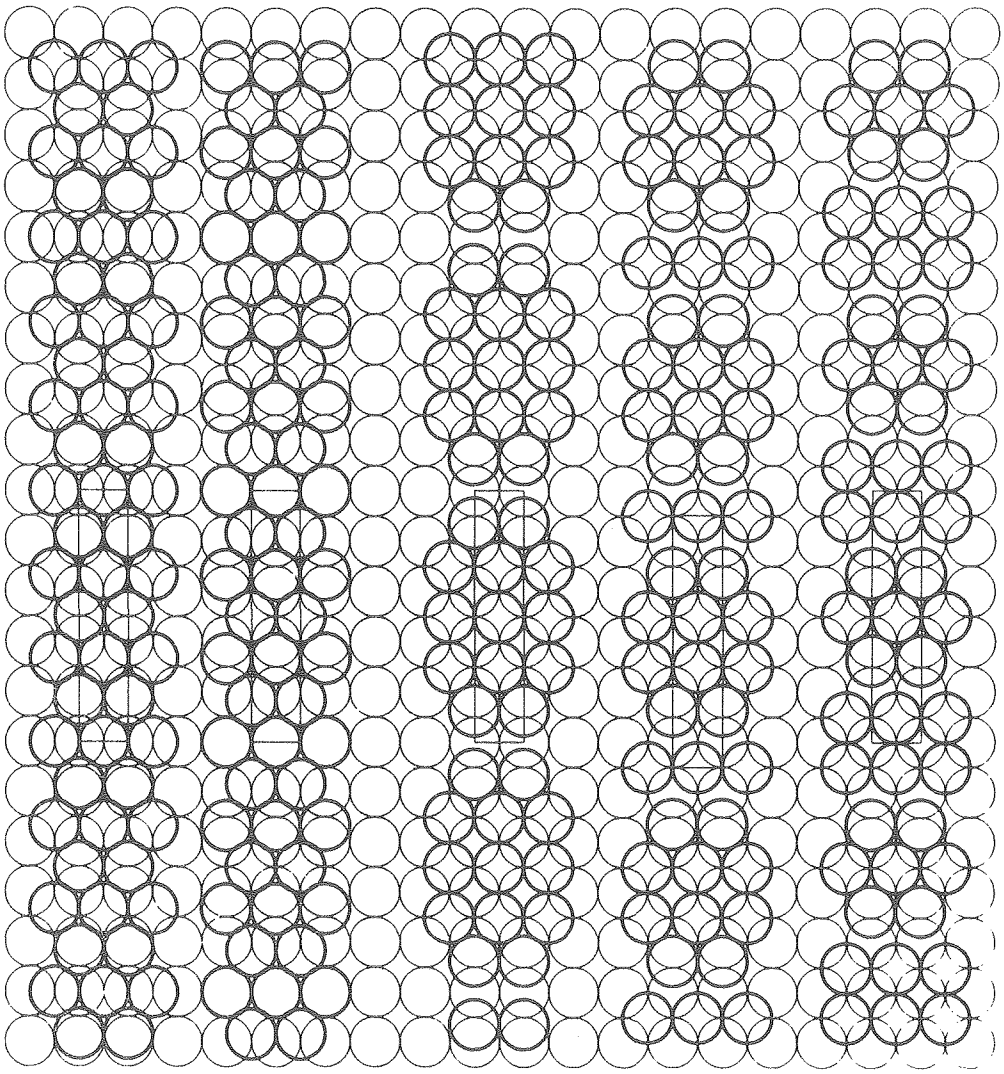

XBL 7912-13737

Fig.11

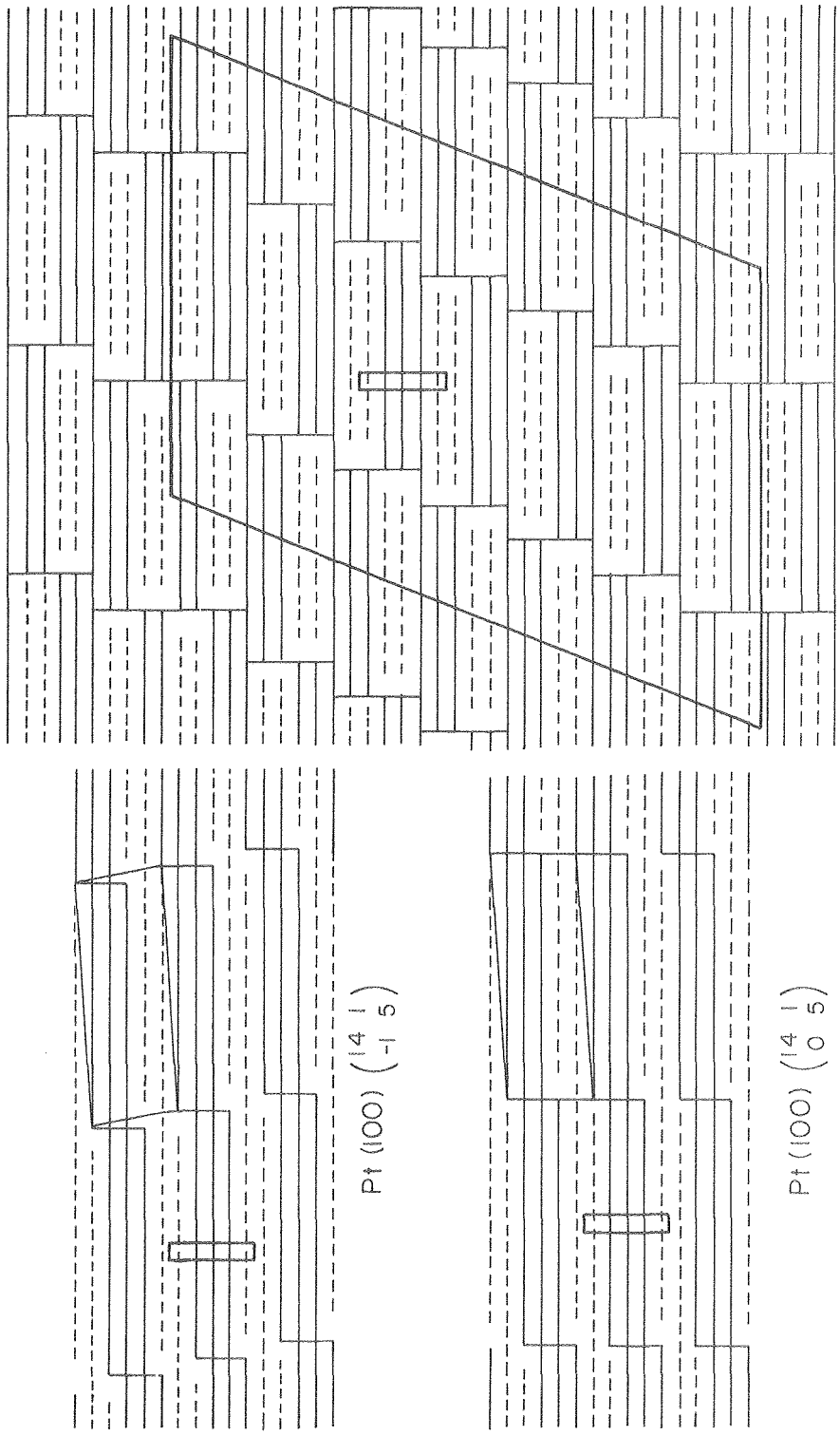
Au (100) c(26x68)
Pt (100) $\begin{pmatrix} 14 & 1 \\ -1 & 5 \end{pmatrix}$
Pt (100) $\begin{pmatrix} 14 & 1 \\ 0 & 5 \end{pmatrix}$
XBL801-4535

Fig. 12

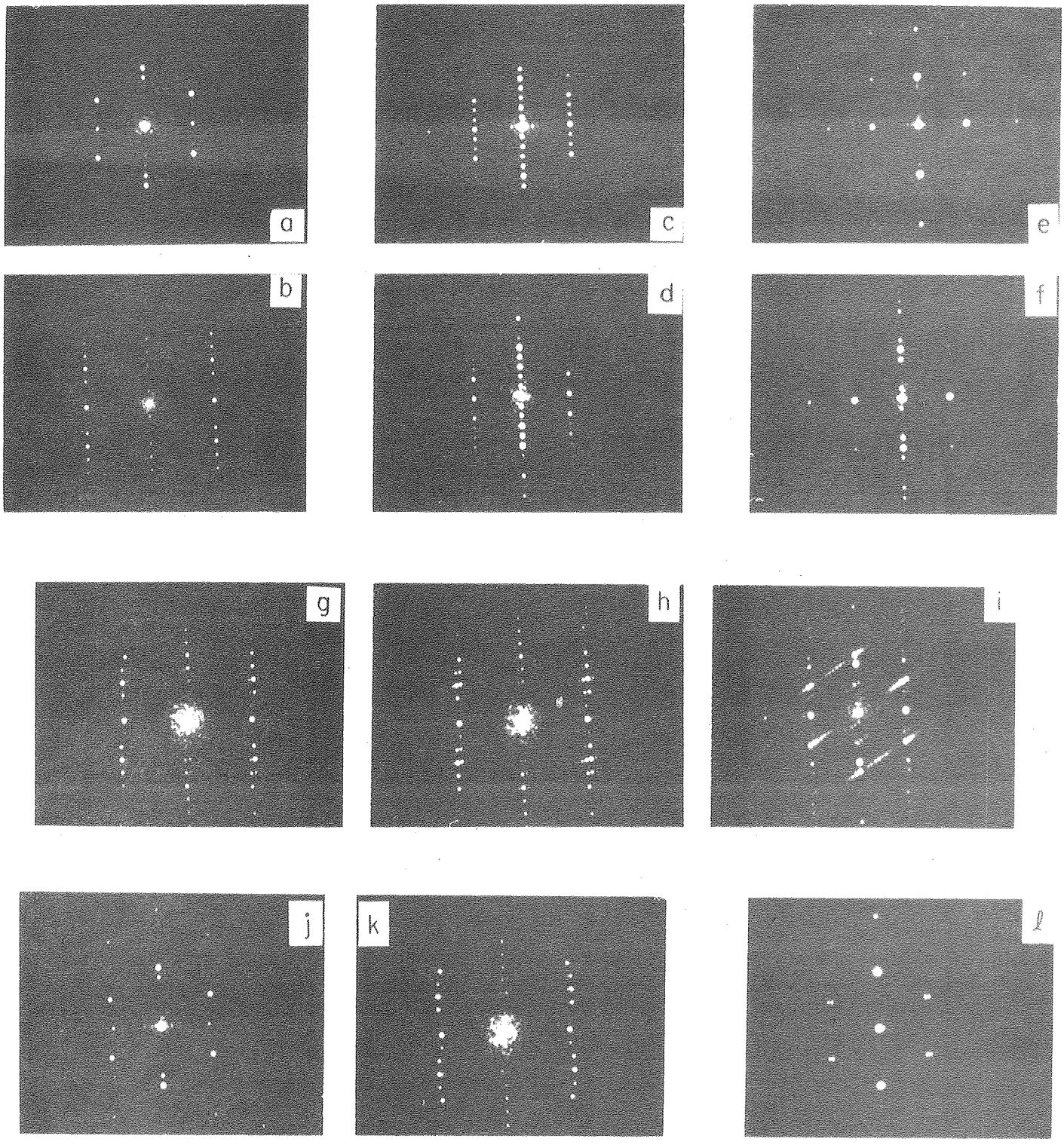

XBB 790-16402

Fig.13